Quantitative evaluation of the decarburization and microstructure evolution of WC–Co during plasma spraying

Qing Zhan [a,b], Ligen Yu [c], Fuxing Ye [a], Qunji Xue [b], Hua Li [b,*]

[a] *School of Materials Science and Engineering, Tianjin University, Tianjin 300072, China*
[b] *Division of Surface Engineering, Ningbo Institute of Materials Technology and Engineering, Chinese Academy of Sciences, Ningbo 315201, China*
[c] *School of Mechanical and Aerospace Engineering, Nanyang Technological University, Singapore 639798, Singapore*

ABSTRACT

The major hurdle that limits extensive application of thermal sprayed WC–Co coatings is the undesirable phase changes from WC to W_2C or even W due to loss of carbon. This study investigated quantitatively the decarburization of WC in both in-flight and coating formation stages during atmospheric plasma spraying. The microstructure evolution of WC particles accompanying the decarburization was also investigated. Results showed that decomposition and oxidation of WC to W_2C predominantly occurred in the in-flight stage (75.82%), while remnant 24.18% occurred during the coating formation stage. Further carbon loss during the coating formation stage of WC–Co droplets is dependent significantly on the temperature of the substrate/pre-coating. Most of the irregular WC particles turned into rounded morphology with a significant decrease in size. W_2C precipitated from the liquid matrix showed either columnar growth or epitaxial growth on WC substrate.

© 2012 Elsevier B.V. All rights reserved.

1. Introduction

Thermal sprayed WC–Co coatings, containing hard brittle WC grains with ductile Co binder, have been widely employed for high wear and abrasive applications [1–3]. However, thermal spray is a high temperature process, usually triggering inevitable phase decomposition and decarburization of WC during coating deposition. A part of WC is transformed into W_2C and metallic tungsten [4], while another part is dissolved in cobalt matrix forming an amorphous compound or precipitated as M_6C and $M_{12}C$ [5] (M_6C and $M_{12}C$ refer to η phases, M_6C: varies from $Co_{3.2}W_{2.8}C$ to Co_2W_4C, $M_{12}C$:Co_6W_6C). The extent of these transformations is dependent on feedstock characteristics and spraying parameters [6,7]. WC phase is desired in the coating, since compared to W_2C, WC has higher wear resistance and other superior properties. The phases that resulted from the transformations and their locations directly affect the properties of the coating. Therefore, prevention or mitigation of the decarburization of WC during thermal spraying has attracted extensive research efforts from the thermal spray research community. However, prior to achieving that goal, a comprehensive understanding of the decarburization phenomenon is essential, which provides the possibility of controlling the phases in WC–Co coatings.

Decarburization mechanisms have been extensively investigated. At elevated temperatures, decarburization comprises the following four major reversible reactions [8]:

$$2WC + O_2 \Leftrightarrow W_2C + CO_2 \tag{1}$$

$$2W_2C + O_2 \Leftrightarrow 2W_2(CO) \tag{2}$$

$$W_2(CO) \Leftrightarrow 2W + CO \tag{3}$$

$$2WC \Leftrightarrow W_2C + C \tag{4}$$

The WC phase undergoes a degradation process to produce W_2C, which subsequently transforms to metallic W when high temperature is attained in an oxygen-rich atmosphere [9]. It is believed that during thermal spraying, carbon diffuses from WC into the matrix and Co diffuses from the matrix into the carbide, forming Co_2W_4C or Co_6W_6C [10]:

$$4Co + 4WC + O_2 \Leftrightarrow 2Co_2W_4C + 2CO \tag{5}$$

$$3Co + 3WC + O_2 \Longleftrightarrow Co_3W_3C + 2CO \qquad (6)$$

$$12Co + 12WC + 5O_2 \Longleftrightarrow 2Co_6W_6C + 10CO \qquad (7)$$
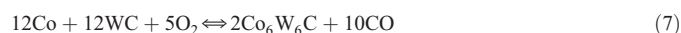
It was evidenced that reactions (1) through (4) take place on the surface of WC particles, but reactions (5) through (7) could only occur when sufficient WC has dissolved in the liquid phase [11]. During thermal spraying, feedstock particles usually experience two stages, namely in-flight stage and coating formation stage. Although phase transformation and microstructural evolution in thermal sprayed WC–Co coatings has been well studied [12–14], it is not clear yet which stage is mainly responsible for the phase changes that WC experiences. It has been well acknowledged that impingement and subsequent splashing–solidification of droplets and accumulation of splats have a negligible effect on pre-splats in terms of phase composition and microstructure. However, the extent to which the phase changes in WC–Co during the coating formation stage is not well established yet. Any processing optimization for controlling the phases in thermal sprayed WC–Co coatings could be possible only when the knowledge of the spray-stage-dependent decarburization of WC becomes sufficient. In addition, phase changes always accompany alteration of microstructure in thermal sprayed coatings. Previous studies have reported that decarburization of WC brought about significant changes in structure [15,16]. The carbides usually turned into a rounded morphology with W_2C shells surrounding WC [17]. However, the knowledge of decarburization-induced microstructure evolution of WC–Co during the high temperature processing is still lacking. Even though intense research effort has been devoted to understanding the decarburization mechanisms during thermal spray, they are still far from a final verdict yet. In the present study, to achieve significant decarburization of WC, atmospheric plasma spray (APS) was employed for WC–Co coating deposition. For comparison purpose, as-sprayed powders were also collected in liquid nitrogen (LN) and room-temperature distilled water. Microstructure of both the powders and the coatings were characterized to understand the phase transformation mechanisms. The decarburization of WC during the in-flight stage and coating formation stage was quantified separately using the Rietveld refinement approach.

2. Materials and testing methods

The commercial agglomerated and sintered WC-12 wt.% Co powders (H.C. Starck, Germany) were used in this study (Fig. 1). The particle size range is $-45 + 15$ μm containing angular WC grains with a mean size range of 1–2 μm, which are embedded in cobalt binder phase. The original weight percentage of C element is 5.38%. The APS-2000 K plasma spray system was employed for the coating deposition on 304 stainless steel plates (dimension: 10 mm × 20 mm × 2 mm). To achieve severe decarburization of the powders, the spray parameters that ascertain full melt state of the WC–Co powders were used (Table 1). For the coating deposition, the substrates were surface polished in order to make the bulk coatings peel off easily. Prior to spraying, ultrasonic cleaning in acetone was conducted for the substrates. In order to investigate the effect of substrate temperature on phase transformation of WC during the coating formation stage, the substrate (100 mm in length) was half immersed in LN (-196 °C). The WC–Co powders were also sprayed directly into LN and room-temperature distilled water with the same spraying parameters.

X-ray diffraction (XRD, Bruker AXS, Germany) was used to detect the phases of the samples at a scanning rate of 0.1°/s using monochromatic Cu-K_α radiation operated at 40 kV. Contents of the phases in the samples were quantified from their XRD spectra using the Rietveld refinement approach. The corresponding Rietquan program is a publicly shared software [18]. The least-squares refinement program employs directly the profile intensities obtained from XRD step-
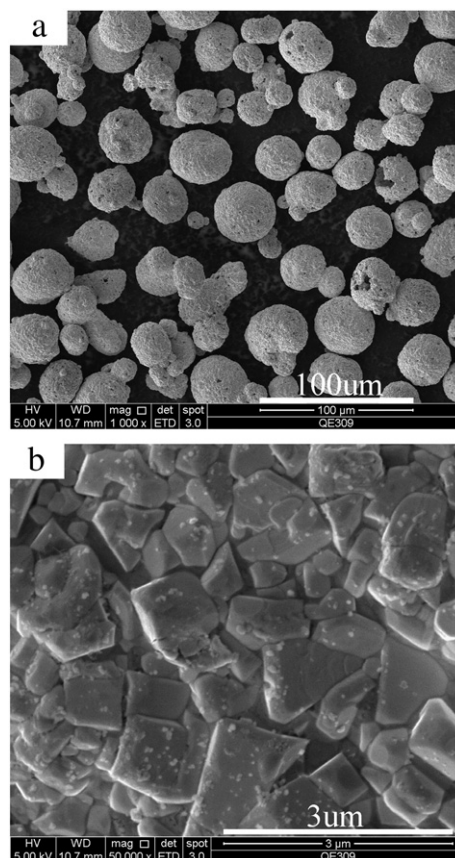
Fig. 1. FESEM images of the agglomerated spherical WC–12Co powders ($-45 + 15$ μm) (a), a higher magnification of the image (b) shows the angular WC particles (1–2 μm).

scanning measurements of the samples instead of the integrated quantities. Acceptance of the calculated data from the XRD patterns was assured by the goodness of fit. In the present study, the refinement with the factor less than 1.3 (1.0 is the best goodness of fit) was adopted. Microstructural features of the samples were characterized using a field emission scanning electron microscope (FESEM, FEI Quanta FEG250, Netherlands). Both surfaces and cross sections of the samples were examined using secondary electrons and backscattered electron signals. Element analysis was also performed using the energy dispersive system (EDS) equipped in the FESEM.

3. Results and discussion

3.1. Decarburization of WC during the in-flight stage

As-plasma-sprayed WC–Co powders were collected by spraying the powders into distilled water and LN. The distance between the gun nozzle exit and the water/LN surface is 140 mm, which is the same as the spray distance for the coating deposition. XRD patterns of the powders indicate marked differences in terms of extent of decarburization of WC during the spraying (Fig. 2). Rietveld refinement

Table 1
Plasma spray parameters.

Primary gas, Ar (l/min)	42
Secondary gas, H_2 (l/min)	11
Powder carrier gas, Ar (l/min)	4
Net energy (kW)	20
Powder feed rate (g/min)	46
Spray distance (mm)	140
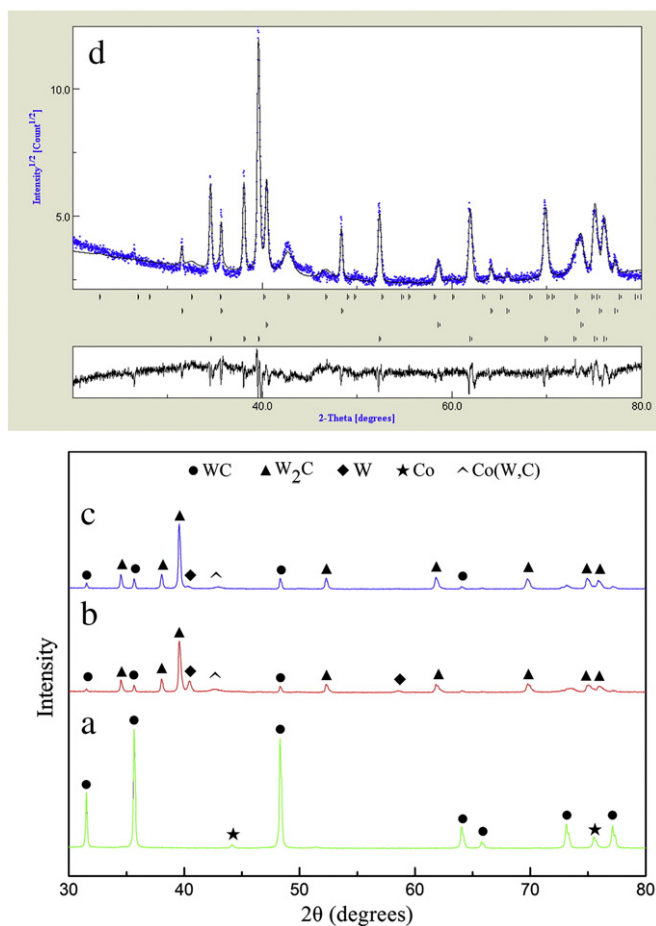
Fig. 2. XRD spectra of the WC–12Co powders ((a) original powders, (b) the powders sprayed in distilled water, and (c) the powders sprayed in liquid nitrogen) and the Rietveld refinement curve of the powders collected in distilled water (d).

of the powders collected in distilled water is also typically shown in Fig. 2d. It is clear that significant decarburization occurred for the particles during the in-flight stage. The peaks assigned to WC were largely weakened (Fig. 2b, c vs. Fig. 2a), while W_2C becomes the major component. The cobalt peaks are not detected in either of the two patterns, suggesting that most of the cobalt is retained in nanocrystalline or amorphous state, a solid solution composed of Co, W and C [19]. Metallic W also appears in the as-sprayed powder, more obviously in the powders collected in distilled water. Rietveld refinement of the XRD patterns gives quantitative evaluation of the phases present in the powders (Fig. 2d, Rietveld refinement curves for other samples are not shown here). The contents of the phases detected in the samples are listed in Table 2 (Rietveld refinement results of the coatings are also shown). Due to the extremely low temperature of LN, the cooling media for the molten WC–Co particles, it is

postulated here that phase changes in the WC–Co particles terminated as soon as they were immersed in LN. Therefore, the XRD detection results of the powders collected in LN give clear information about the extent of phase transformation of WC–Co during the in-flight stage. A total of 71.03% of WC particles lost their carbon (25.49% vs. 88.00% in the original powders) during the in-flight stage. Based on this data, it is clear that the dwelling of the sprayed powders in room-temperature water contributes to the further enhanced decarburization (14.87%) of the WC particles (12.40% vs. 25.49% of the original 88.00% WC in the feedstock powders). Apart from the further decomposition of WC, there is a significant increase in the relative content of metallic W (from 1.55% to 6.44%) and η phases (Co_6W_6C/Co_3W_3C, from 11.11% to 40.63%). This phenomenon gives insight into the possible mechanism that further decarburization of W_2C to W and formation of the η phase presumably occur during the coating formation stage, while the contribution of the in-flight stage plays a minor role.

3.2. Decarburization of WC during coating formation stage

To further quantitatively evaluate contributions of the in-flight stage and the coating formation stage to the decarburization of WC, WC–Co coatings were also deposited and characterized. It is well known that penetration depth (valid detection depth) of traditional XRD is usually less than 10 μm. Therefore, the XRD spectrum detected from the bottom side of the coating provides phase information of its first layer. XRD spectra of the coatings (Fig. 3) exhibit similar results due to the good cooling condition attained by LN cooling. However, there are some small humps in the 2θ range of 37–47° in the spectrum for the top layer, which are assigned to Co_3W_3C and Co_6W_6C. A much broader diffraction halo exists in the same 2θ range for the bottom layer, suggesting a nanocrystalline-amorphous structured binder phase. The WC peaks for the top layer are weaker than those for the bottom layer. The W_2C phase shows strong peak intensity. Rietveld refinement (Table 2) suggests slightly enhanced decarburization of WC in the top layer compared to that which happened in the first layer of the coatings (7.75% vs. 5.56%). W is detected in the top layer (2.81%), while it is absent in the bottom layer. In addition, there is a marked difference in the content of the η phase (Co_6W_6C/Co_3W_3C) (16.62% vs. 3.58%). The first layer of the coating was formed by rapid solidification with an extremely high cooling rate of the flattened droplets after the particles impacted on the substrate surface. Even though the temperature of the substrate before the coating deposition was not measured directly, based on the fact that sufficient cooling of the substrate was ensured prior to spraying, it was believed that the substrate temperature for first-layer deposition is close to that of LN. The XRD result (Fig. 3a) suggests major phase changes for the WC–Co particles during their in-flight stage. For the top layer of the coating, since the coating formation is an accumulation process by individual splats, even though the substrate was half-immersed in LN during coating deposition, heat transfer from successive splats inevitably gives rise to continually increased temperature of the pre-coating. It was well understood that temperature profile through the layers would have a maximum at a location close to the top side of the coating [20]. The temperature of the substrate/pre-coating

Table 2
Rietveld refinement results (wt.%) for the samples.

Sample	Phase				
	WC	W_2C	W	Co_6W_6C/Co_3W_3C	Total C element (calculated)
Powder collected in distilled water	12.40 ± 0.41	40.54 ± 0.05	6.44 ± 0.13	40.63 ± 1.51	2.37
Powder collected in LN	25.49 ± 0.48	61.84 ± 0.02	1.55 ± 0.11	11.11 ± 1.14	3.60
Bottom side of the coating deposited on the LN-cooled substrate	7.75 ± 0.43	88.67 ± 0.07	–	3.58 ± 0.44	3.30
Top side of the coating deposited on the LN-cooled substrate	5.56 ± 0.47	75.01 ± 0.02	2.81 ± 0.23	16.62 ± 2.58	2.84
Original powder	88.00	–	–	–	5.39
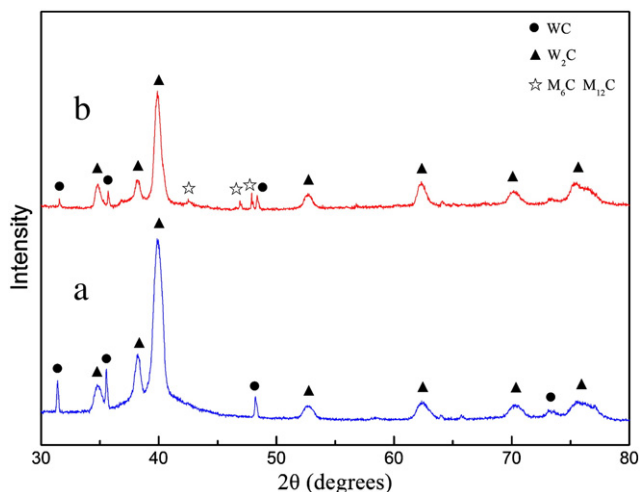
Fig. 3. XRD patterns of the APS WC–Co coating detected from (a) the bottom side of the coating, and (b) the top side of the coating. M_6C and $M_{12}C$ refer to η phases, M_6C: varies from $Co_{3.2}W_{2.8}C$ to Co_2W_4C, $M_{12}C$:Co_6W_6C.

was measured using an infrared thermometer (ST60, Raylek). It was found that immediately after the coating deposition, the coating surface temperature reached 300 °C. The reduced cooling rate brought about more time for the carbides to precipitate from the matrix. The consequently reduced heat conduction for the top layer should be responsible for the further decarburization and formation of the metallic W and η phases.

Since all the samples were made with the same spray parameters, the extent of the decarburization is considered identical during the particles' in-flight stage. The different contents of the phases in the sprayed powders reflect the influence of cooling conditions on the phase transformation. Compared with the powders collected in LN, water-cooled powders have undergone severer decarburization. Calculation of total carbon in the samples (Table 2) suggested a significant drop from the original 5.38% to 2.37%, much less than that of the powders collected in LN (3.60%), indicating further oxidation and decarburization during the solidification stage of the powders. The significant carbon loss can also explain the presence of high percentage metallic W and Co_6W_6C in the samples, since it was pointed out that the precipitation of carbides and metallic W is driven not only by temperature but also by carbon concentration in the matrix [19]. Based on the results obtained from both the powders and the coatings, it can be concluded that the phases, i.e. W and Co_6W_6C, are mainly formed during the coating formation stage. Absence of W in the bottom layer of the coating further verifies the postulation that the extent of the decarburization of the powders collected in LN approximately represents the overall decarburization of WC which occurred during the in-flight stage. Compared to the powders collected in LN, the bottom layer of the coating showed a certain amount of oxidation due to the larger surface area of the flattened droplets, as suggested by the difference in carbon content (3.3% vs. 3.6%). In addition, there was a significant decrease in WC content (7.75% vs. 25.49%) and a simultaneous increase in W_2C (88.67% vs. 61.84%). The protective atmosphere of volatile nitrogen can be ignored since LN was also used during the coating deposition. During the coating formation stage, rapid flow of the liquid matrix (droplets) would be beneficial for dissolving WC and consequently homogenizing the composition in particular the carbon concentration of the splats. W_2C is easier to precipitate from the matrix rather than from metallic W and η phases. The liquid matrix also opts to directly turn into a nano-amorphous binder phase if cooling rate is high enough [21]. It should be noted, however, that the Rietveld method only prevails for crystalline
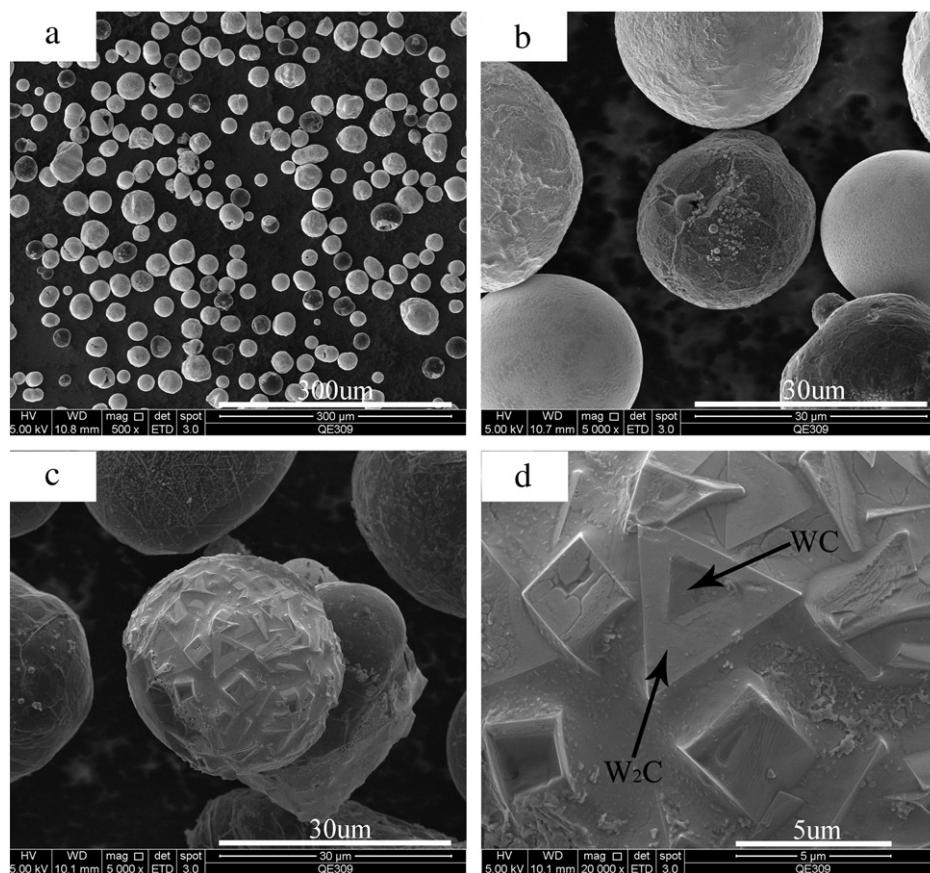
Fig. 4. Topographical morphology of the as-sprayed WC–Co powders showing different contrasts (a, b) and undissolved carbides with direct transformation of WC to W_2C (c, d).

coatings. The use of this approach in determining amorphous fraction is very limited [22].

3.3. Microstructure evolution of WC–Co during plasma spraying

To further elucidate the mechanisms of the decarburization of WC–Co powders during plasma spray, microstructure evolution of the powders was also characterized. After being sprayed into LN, the particles become ideally spherical, denser and have a smoother surface (Fig. 4), as compared to the starting powders (Fig. 1). Cross-sectional morphological view of the sprayed particles has suggested complete melting of the particles (data not shown here). Observation of the sprayed particles has proven to be an effective approach for evaluating the melt state of the sprayed particles [23]. The powders exhibit different contrasts at their surfaces (Fig. 4a, b), which is very likely attributed to different molten state and phase compositions. The particles exhibiting bright color (Fig. 4b) suggest a well-molten state. EDS analysis revealed that the atomic C/W ratio of the powders in dark contrast is ~2.4, much higher than the original value for the starting powders, 1.0. It is known that sprayed particles experience heterogeneous heating in the plasma jet [24]. The powders exhibiting bright color might have passed through the center of the plasma jet where oxidation was prevented by the inert Ar. Meanwhile, the shell of the droplets encountered the highest temperature in the plasma jet [25], which greatly promoted the dissolution of WC particles. Owing to their relatively high solubility, C and W diffused from the inner part towards the surface of the particles. C atoms diffused much more rapidly than W, giving rise to gradually increased C/W ratio at the particle surface. The particles in bright color (Fig. 4a, b) showed a low atomic C/W ratio (0.15), indicating severe decarburization in these regions. These particles might have passed through the outer flame where the temperature is not high enough to melt them completely. Many undissolved angular WC grains can also be seen on their surfaces (Fig. 4c). EDS analyses suggest that the atomic C/W ratio at the inner part of the grains (0.84) is close to the original value of WC (1.0), while the ratio at the outer part is much lower (0.43), indicating that the rim of the WC grains transformed to W_2C (Fig. 4d). The brighter color exhibited by the outer shell also suggests a higher W content. The multiple phases detected on the WC grains are justified by the phenomenon that the periphery of the plasma jet contacted fully with the oxygen which directly reacted with WC [26]. An in-situ transformation of WC into W_2C occurred and might be followed by further oxidation of sub-carbides [8]. To fully understand the topographical feature of the powders, cross-sectional morphology of the powders was also analyzed from the FESEM images in BSE mode (Fig. 5). It is clear that the original angular shape of the carbide grains turned morphologically round, most likely due to the dissolving process, with the particle size being dramatically decreased into submicron range (~500 nm). The carbides exhibit a very bright contrast, indicating a high relative content of W. This has been confirmed by EDS analysis (average atomic C/W ratio: 0.16). The atomic percentage of Co diffused from the matrix varies from 12.5% to 18.5%. Carbon diffused from the WC grains into matrix and got oxidized at the particle surface.

Morphology of the coatings gives further insight into the decarburization mechanism and microstructure evolution (Fig. 6). For cross-sectional morphology observation, the coatings were directly snapped off without polishing. The fresh fractured coatings show a typical columnar structure near their bottom side (Fig. 6a, b), with the growth direction being in accordance with the temperature gradient. The morphological feature suggests that this structure was formed by the precipitation of phases from the liquid matrix as the droplet rapidly cooled down during its flattening and solidification. EDS analyses of the columnar-shaped splats showed an average C/W ratio of 0.42, being close to that of W_2C, with a very low percentage of Co (3.3%). Since the XRD detection has shown little amount of η phase in the bottom side of the coating (Fig. 4a), it is believed that these columnar crystals are mainly composed of W_2C. W_2C might have nucleated during the in-flight stage and grew rapidly upon quenching of droplets.
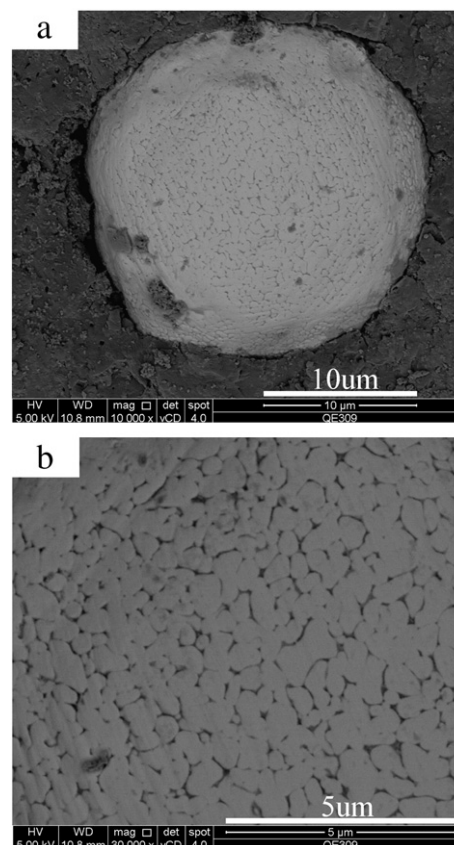
Fig. 5. BSE images of the cross-sections of the LN-cooled WC–Co particles showing decreased size and rounded morphology of the WC grains with mass dissolution of Co.

For the particles that have not suffered severe decarburization in the plasma jet, their WC grains encountered minor changes and retained their original morphology (Fig. 6c). Still many small micropores in WC particles are observed as a result of diffusion and oxidation of carbon, as can be more clearly seen in Fig. 6d. The polished cross-sectional microstructure of the coating (Fig. 7) indicates two specific features of the WC grains: smaller WC grains (less than 1 μm) near the splat periphery and bigger WC grains (~2 μm) close to the splat center. High temperature and direct contact with oxygen brought about dissolution, decomposition and decarburization of WC, which further triggered reduced WC grain size at the edge of the splats. The internal WC grains experienced lower temperature and less degree of oxidation, leading to minor changes in their structure and morphology. Furthermore, WC grains are always noted of being surrounded by shells or small globular particles. It is believed that the rim around the WC particles contains a W_2C phase and the epitaxial growth of W_2C on the WC substrate has been reported [14,19,27]. The columnar morphology of W_2C (Fig. 7) indicates that W_2C grains are formed by precipitation of the phase from the liquid matrix. The composition of the matrix is close to M_2C which resulted from decarburization during the splat quenching. The interface between WC grains acts as a favorable nucleation site and promotes the epitaxial growth of W_2C [28]. Metallic W and η phases could also precipitate depending on local carbon concentration in the liquid matrix and cooling condition as well. Further study on the effect of the structural features on mechanical performances of the coatings is being conducted.

4. Conclusions

Phase transformation of WC to W_2C during plasma spraying of WC–Co powders predominantly occurred during the in-flight stage (75.82% of overall transformation exhibited by the WC–Co powders). W_2C was formed by direct oxidation or decomposition of WC grains
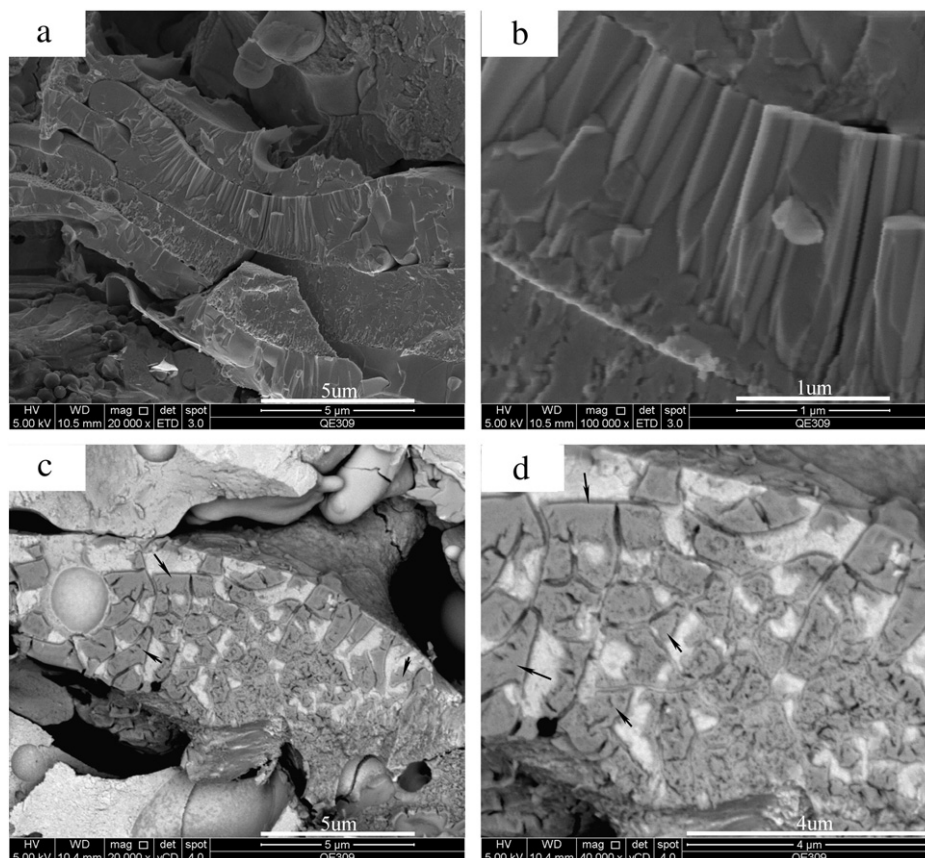
Fig. 6. Cross-sectional morphology of the bottom layer of the WC–Co coating (deposited on the LN-cooled substrate) showing the columnar W_2C crystals (a, b), the BSE images show clearly the retained WC grains in the splat (c and d, WC grains are dark in color, black arrows point to representative WC grains). (for a and b, temperature gradient is from the top to the bottom).

and retained the faceted morphology on particle surfaces. Dissolution of internal WC particles into molten Co matrix brought about morphological changes of WC grains, i.e. from an original angular shape to a rounded shape, accompanied with a significant decrease in size (1–2 μm to 500 nm). The coating formation stage is responsible mainly for further carbon loss as a result of the formation of W and η phases. Carbon loss during the coating formation stage of the WC–Co droplets is dependent significantly on the temperature of the substrate/pre-coating, 11.76% of the coating was deposited on the LN-cooled substrate and 18.04% of the coating was deposited on the 300 °C pre-coating. W_2C precipitated from the liquid matrix, exhibiting

columnar growth or epitaxial growth on WC substrate depending on local nucleation conditions.

Acknowledgment

References

[1] D.M. Kennedy, M. Helali, M.S.J. Hashmi, Surf. Coat. Technol. 68–69 (1994) 477.
[2] P. Chivavibul, M. Watanabe, S. Kuroda, K. Shinoda, Surf. Coat. Technol. 202 (2007) 509.
[3] J. He, J.M. Schoenung, Surf. Coat. Technol. 157 (2002) 72.
[4] P. Mazars, D. Manesse, Mater. Sci. Eng. 88 (1987) 21.
[5] V. Ramnath, N. Jayaraman, Mater. Sci. Technol. 5 (1989) 382.
[6] M.E. Vinayo, F. Kassabji, J. Guyonnet, P. Fauchais, J. Vac. Sci. Technol. A 3 (1985) 2483.
[7] S. Rangaswamy, H. Herman, Advances in Thermal Spraying, Pergamon Press, Oxford, 1986.
[8] C.J. Li, A. Ohmori, Y. Harada, J. Mater. Sci. 31 (1996) 785.
[9] D. Tu, S. Chang, C. Chao, C. Lin, J. Vac. Sci. Technol. A 3 (1985) 2479.
[10] D. Lou, J. Hellman, D. Luhulima, J. Liimatainen, V.K. Lindroos, Mater. Sci. Eng. A 340 (2003) 155.
[11] W.D. Swank, J.R. Fincke, D.C. Haggard, G. Irons, R. Bullock, Thermal Spray Industrial Applications, ASM International, Boston, 1994, p. 319.
[12] J.E. Nerz, B.A. Kushner, A.J. Rotolico, J. Therm. Spray Technol. 1 (1992) 147.
[13] E. Sanchez, E. Bannier, M.D. Salvador, V. Bonache, J.C. Garcia, J. Morgiel, J. Grzonka, J. Therm. Spray Technol. 19 (2010) 964.
[14] S. Thiele, K. Sempf, K. Jaenicke-Roessler, L.-M. Berger, J. Spatzier, J. Therm. Spray Technol. 20 (2011) 358.
[15] P.S. Babu, B. Basu, G. Sundararajan, Acta Mater. 56 (2008) 5012.
[16] N.S. Lim, S. Das, S.Y. Park, M.C. Kim, C.G. Park, Surf. Coat. Technol. 205 (2010) 430.
[17] J.M. Guilemany, J.M. de Paco, J. Nutting, J.R. Miguel, Metall. Mater. Trans. A 30 (1999) 1913.
[18] R.A. Young, The Rietveld Method, Oxford University Press, Oxford, 1995.
[19] C. Verdon, A. Karimi, J.L. Martin, Mater. Sci. Eng. A 246 (1998) 11.
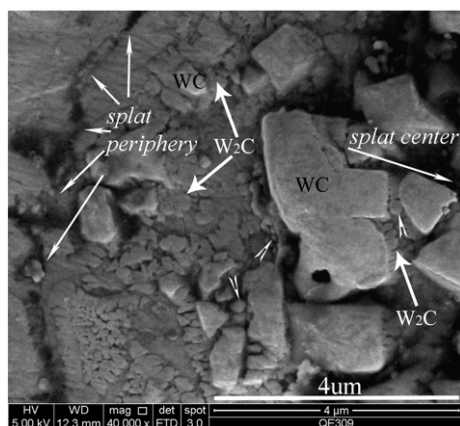
Fig. 7. Typical cross-sectional FESEM morphology of the APS WC–Co coating showing epitaxial growth of W_2C on WC substrate (hollow arrow head points to small globular particle surrounding the WC grains).

Q. Zhan et al. / Surface & Coatings Technology 206 (2012) 4068–4074

[20] V.V. Sobolev, J.M. Guilemany, J.A. Calero, J. Mater. Process. Technol. 96 (1999) 1.
[21] A.H. Dent, S. DePalo, S. Sampath, J. Therm. Spray Technol. 11 (2002) 551.
[22] L. Lutterotti, R. Ceccato, R. Dal Maschio, E. Pagani, Mater. Sci. Forum 278–281 (1998) 98.
[23] H. Li, K.A. Khor, P. Cheang, Mater. Sci. Eng. A293 (2000) 71.
[24] P. Fauchais, M. Vardelle, Pure Appl. Chem. 66 (1994) 1247.
[25] E. Pfender, Pure Appl. Chem. 57 (1985) 1179.
[26] J. Subrahmanyam, M.P. Srivastava, R. Sivakumar, Mater. Sci. Eng. 84 (1986) 209.
[27] H. Li, K.A. Khor, L.G. Yu, P. Cheang, Surf. Coat. Technol. 194 (2005) 96.
[28] D.A. Stewart, P.H. Shipway, D.G. McCartney, Acta Mater. 48 (2000) 1593.